RSC Advances

PAPER

View Article Online
View Journal | View Issue

Cite this: *RSC Adv.*, 2023, **13**, 2635

Serum metabolomics strategy for investigating the hepatotoxicity induced by different exposure times and doses of *Gynura segetum* (Lour.) Merr. in rats based on GC-MS†

Ying Li,‡[a] Yingxin Tian,‡[ab] Qixue Wang,[a] Xinyi Gu,[a] Long Chen,[c] Yiqun Jia,[c] Shan Cao,[d] Ting Zhang, *[a] Mingmei Zhou *[a] and Xiaojun Gou*[d]

Gynura segetum (Lour.) Merr. (GS), has been widely used in Chinese folk medicine and can promote circulation, relieve pain and remove stasis. In recent years, the hepatotoxicity caused by GS has been reported, however its mechanism is not fully elucidated. Metabolomic techniques are powerful means to explore the toxicological mechanism and therapeutic effects of traditional Chinese medicine. The purpose of this study was to establish a serum metabolomics method based on Gas Chromatography-Mass Spectrometry (GC-MS) to explore the hepatotoxicity mechanism of different exposure times and doses of GS in rats. Sprague Dawley (SD) rats were administered daily with distilled water, 7.5 g kg^{-1} GS, or 15 g kg^{-1} GS by intragastrical gavage for either 10 or 21 days. The methods adopted included enzyme-linked immunosorbent assay (ELISA), Hematoxylin and Eosin (H&E) staining and GC-MS-based serum metabolomics. Serum biochemistry analysis showed that the levels of alanine aminotransferase (ALT), aspartate aminotransferase (AST), triglycerides (TG), total bilirubin (TBIL) and total bile acid (TBA) significantly ($P < 0.05$) increased while the levels of albumin (ALB) and high-density lipoprotein (HDL) significantly ($P < 0.05$) decreased in GS-treated groups, compared with the control group. Interestingly, the ALT, AST, TG and ALB levels changed in a time- and dose-dependent manner. The results of H&E staining showed the degree of liver damage after administration of GS gradually deepened with the extension of administration time and the increase of the dose. According to the results of metabolomics analysis, 26 differential metabolites were identified, which were involved in 8 metabolic pathways including phenylalanine metabolism, glyoxylic acid and dicarboxylic acid metabolism and so on. Meanwhile, the number of differential metabolites in different GS-treated groups was associated with GS exposure time and dose. Therefore, we concluded that GS might induce hepatotoxicity depending on the exposure time and dose.

Received 16th November 2022
Accepted 18th December 2022

DOI: 10.1039/d2ra07269f

rsc.li/rsc-advances

1 Introduction

Gynura segetum (Lour.) Merr., called Tusanqi in China, is a plant of the Asteraceae family.[1] It has been widely used in Chinese folk medicine and can promote circulation, relieve pain and remove stasis.[2] The chemical components of GS mainly include alkaloids, flavones, coumarins and triterpenes, *etc.*[3] GS is applied clinically in the treatment of cancer, inflammation, diabetes, hypertension and skin afflictions.[4] However, GS contains pyrrolizidine alkaloids (PAs), which are the most hepatotoxic natural chemicals.[5,6] The intake of PAs has been regarded as one of the major causes responsible for the development of hepatic sinusoidal obstruction syndrome (HSOS), a kind of liver disease with hepatomegaly, ascites and weight gain.[7] And in recent years, HSOS caused by GS has been increasingly reported in China.[2,5,8,9]

PAs are metabolized to pyrrolic ester metabolites by the liver cytochrome P450 enzymes and further induce hepatotoxicity by reacting with cellular proteins and DNA.[10] The dysregulation of cellular redox balance occurred in PAs-treated rats,[11] suggesting that mitochondria might be involved in PAs-induced hepatotoxicity. A study further proved that GS caused hepatotoxicity by

[a]*Institute of Interdisciplinary Integrative Medicine Research, Shanghai University of Traditional Chinese Medicine, Shanghai, 201203, China. E-mail: zhtcpu@hotmail.com; zhoumm368@163.com*

[b]*School of Pharmacy, Shanghai University of Traditional Chinese Medicine, Shanghai, 201203, China*

[c]*Experiment Center of Science and Technology, Shanghai University of Traditional Chinese Medicine, Shanghai, 201203, China*

[d]*Central Laboratory, Baoshan District Hospital of Integrated Traditional Chinese and Western Medicine of Shanghai, Shanghai, 201999, China. E-mail: gouxiaojun1975@163.com; Tel: +86 21 56601100. Fax: +86 21 36072150*

† Electronic supplementary information (ESI) available. See DOI: https://doi.org/10.1039/d2ra07269f

‡ These authors contributed equally to this work.

dysregulating mitochondrial ROS generation *via* a SIRT3-SOD2 pathway.[12] In addition, the expression of matrix metalloproteinase-9 (MMP-9) was increased in blood, lung and liver tissues of GS-treated rats, indicating MMP-9 may play an important role in early pathological changes of HSOS.[13] However, the molecular biological mechanism of hepatotoxicity induced by GS is still not clear.

Metabolomics, one of the disciplines of systems biology, has become a powerful tool in the study of toxicological mechanisms of drugs due to the systemic and dynamic view of the endogenous metabolic profiles.[14,15] Metabolomic analytical platforms used in the majority of studies are nuclear magnetic resonance (NMR), liquid chromatography-mass spectrometry (LC-MS) and gas chromatography-mass spectrometry (GC-MS). Previous researches have shown that metabolomics methods based on LC-MS have been used to investigate hepatotoxicity of GS in rats.[16–18] However, there are no studies on the hepatotoxicity mechanism of the different exposure times and doses of GS based on GC-MS method so far. GC-MS is often considered a necessary complement to LC-MS to have a proper global metabolic profile of a sample, such as increasing the metabolite coverage like sugars, amines, alcohols and amides.[19,20] Moreover, GC-MS somewhat avoids problems in LC-MS such as matrix effects and ion suppression by co-eluting compounds, and thus achieves greater chromatographic resolution.[21]

In this study, we further performed a serum metabolomics method based on GC-MS combined serum biochemical analysis, histopathology to investigate the hepatotoxicity caused by GS of two new exposure times (10 day and 21 day) and dose (7.5 g kg^{-1} and 15 g kg^{-1}) on and to further illuminate toxicological mechanisms of GS.

2 Experiment

2.1 Chemicals and reagents

Methanol, pyridine and methoxyamine hydrochloride in analytical grade were purchased from Sinopharm Chemical Reagent Co., Ltd (Shanghai, China). Ultra-pure water was freshly prepared by a Milli-Q system (Morey Biosciences, Inc., Shanghai, China). BSTFA (1% TMCS) was supplied from REGIS (Regis Technologies, Inc., USA). Nonadecanoic acid and 2-chlorophenylalanine were purchased from Shanghai ANPEL Scientific Instrument Company (Shanghai, China) and Aladdin Biochemical Technology Co., Ltd (Shanghai, China), respectively. ALT, AST, TBIL, TBA, ALB, TG, TCH, HDL and LDL ELISA kits were purchased from Shanghai Huachen Biological Reagent Co., Ltd (Shanghai, China).

2.2 Preparation of drug

Gynura segetum (Lour.) Merr. was obtained from Bozhou (Anhui, China). It was identified as the root of *Gynura segetum* (Lour.) Merr. by Professor Yajun Cui and a representative specimen was stored in the laboratory of Shanghai University of Traditional Chinese Medicine (No. 20180322). The drug was prepared as previous study.[22] The fresh root of *Gynura segetum* (Lour.) Merr were dried at room temperature after washing and slicing. Then 1500 g dried rhizome of GS was crushed. After soaking in 9000 mL distilled water for 2 hours, the solution was boiled for 1.5 h, then filtered, and the boiling process was repeated one more time with 6000 mL distilled water. The filtrate was merged and concentrated to 1000 mL (1 mL of the extract corresponding to 1.5 g of plant material). Before each administration, the high and low concentrations of drug solution were prepared from an appropriate amount of the original solution, which were equivalent to 1.5 g mL^{-1} and 0.75 g mL^{-1} of the crude drug of GS.

2.3 Animal treatments and sample collection

Male SD rats (six-week-old, 180 ± 20 g, no. SCXK 2017-0005) were provided by Shanghai SLAC Laboratory Animal Co., Ltd (Shanghai, China). The entire animal experiment was approved by the Animal Ethics Committee of Shanghai University of Traditional Chinese Medicine (no. PZSHUTCM190621010). Animals were adaptively fed in the animal house (temperature, 20 ± 2 °C; relative humidity, 45–70%; light/dark cycle, 12 h) for 7 days with water and food freely prior to oral administration. Forty-eight rats were randomly divided into the following groups: control group ($n = 16$), low-dose group ($n = 16$) and high-dose group ($n = 16$). Low-dose group and high-dose group: 7.5 g kg^{-1} and 15 g kg^{-1} were intragastrically administrated to each rat daily, respectively. Control group: equal volume distilled water (1 mL/100 g) was intragastrically administrated to each rat daily. After 10 days, half of each group were randomly sacrificed, and the remaining rats were sacrificed after 21 days. The blood samples were collected from the rat abdominal aorta and centrifuged (3500 rpm, 10 min, 4 °C) in 1730R GENESPEED (Gene Co., Ltd, Germany). The serum was stored in the refrigerator at −80 °C until blood biochemical analysis and metabolomics analysis. The liver tissues were removed from rats immediately after sacrifice and stored at −80 °C until H&E staining.

2.4 Serum biochemistry assay

The serum samples taken out from the refrigerator at −80 °C were thawed at 4 °C. Then the constant temperature mixer (Hangzhou Miu Instruments Co., Ltd, Jiangsu, China) was applied to mix serum. According to the kit instruction, serum biochemistry analysis was carried out with 7080 automatic biochemistry analyzer (Hitachi Trading Co., Ltd, Japan), including following parameters: alanine aminotransferase (ALT), aspartate aminotransferase (AST), total bile acid (TBA), total bilirubin (TBIL), triglycerides (TG), total cholesterol (TCH), high-density lipoprotein (HDL), low-density lipoprotein (LDL) and albumin (ALB).

2.5 Histopathology

The liver samples taken out from the refrigerator at −80 °C were thawed at 4 °C and then stored in 10% formaldehyde solution for fixation, embedded in paraffin after dehydration and sectioned into 5 μm sections. Tissue sections were stained with hematoxylin and eosin (H&E), and the liver histopathological

changes were observed under the microscope (200× magnification).

2.6 Metabolomics analysis

The serum samples were thawed at 4 °C and 100 μL from each serum sample was taken to a clean centrifuge tube. Then, 400 μL methanol and 10 μL internal standard (nonadecanoic acid, 2-chlorophenylalanine) were added, mixed in TARGIN™ VX-II Multi-tube vortex oscillator (Beijing Targin Technology Co., Ltd, Beijing, China), and centrifuged (12 000 rpm, 10 min, 4 °C). A 200 μL of supernatant was gathered and dried under concentration and freezing. Thirty microliters of pyridine containing 20 mg mL^{-1} methoxyamine hydrochloride was added, shaked for 10 s and incubated at 37 °C for 1.5 h. Then BSTFA (with 1% TMCS) was injected with a volume of 30 μL, shaked for 10 s, and derivatized in a constant temperature oven (Shanghai Jinghong Experimental Equipment Co., Ltd, China) at 70 °C for 1 h before GC-MS analysis. A quality control (QC) sample was prepared through mixing same volume of each sample.

In GC-MS analysis, an Agilent 7890A GC system with a 7000B QQQ-MS detector (Agilent Technologies Company, CA, USA) were applied to process the derivatized serum samples. We used a VF-WAXms capillary column (30 m × 0.25 mm, 0.25 μm). As the carrier gas, the flow rate of helium was set at 1 mL min^{-1} through the column. The initial oven temperature was held at 80 °C for 2 min, ramped to 300 °C at a rate of 10°C min^{-1}, and finally held at 300 °C for 6 min. The injection volume was 1 μL with splitless. The temperatures of injector and Max Oven Temp were set to 280 °C and 320 °C, respectively. The electron impact ionization (70 eV) was performed within a mass range from 50 to 600 m/z in a full-scan mode, and the equilibration time and the solvent delay time were set to 0.5 min and 5.65 min, respectively.

2.7 Multivariate data analysis and identification of potential biomarkers

The unprocessed raw files were exported into Microsoft Excel, including retention time, peak area, mass-to-charge ratio of each substance detected and sample message. Then the pre-processed data were imported into SIMCA version 14.1 (Umetrics, Umea, Sweden) for multivariate data analysis. Principal component analysis (PCA) and orthogonal partial least squares discriminant analysis (OPLS-DA) were performed to visualize the alterations of metabolic profiling between the GS-treated groups and control groups. As the key parameters in OPLS-DA, the values of R^2X, R^2Y and Q^2 were checked to guarantee the rationality of the experimental model. Permutation test was used to prevent overfitting of the OPLS-DA model. Variable importance in the projection (VIP) values produced in the OPLS-DA model were applied to find differential metabolites, and metabolites with VIP >1 were further processed for Student's t-test by SPSS 21.0 statistical software (IBM, Armonk, NY, USA). According to the above results, FC values were calculated in Microsoft Excel. Finally, metabolites with VIP >1, $P < 0.05$ were considered to be significant differential metabolites.

GC-MS raw data were imported into Agilent Masshunter workstation qualitative software for peak picking and identification, and NIST database was applied to perform identification of the significantly differential metabolites by their m/z, mass spectra and retention time. The identification of potential biomarkers was verified by further searching the Human Metabolome Database (HMDB, **https://www.hmdb.ca/**) and Kyoto Encyclopedia of Genes and Genomes (KEGG, **https://www.kegg.jp/**). Corresponding metabolic pathways were found and drew by MetaboAnalyst 5.0 (**https://www.metaboanalyst.ca/**). Heatmaps were created to visualize the differences between groups of metabolites by using Bioinformatics online tool (**http://www.bioinformatics.com.cn/**).

2.8 Statistical analysis

All data were shown as mean ± standard deviation (SD). The statistical discrepancy between GS-treated groups and control group was evaluated based on the result of Student's t-test in SPSS 21.0 (IBM, Armonk, NY, USA) and $P < 0.05$ represented statistical significance. Additionally, Graphpad Prism 6.0 (GraphPad Software Inc., USA) was applied to visualize the processed data. Spearman's correlation coefficient was performed using SPSS 21.0 and the results were shown with heatmaps by using Bioinformatics online tool.

3 Results

3.1 Serum biochemical analysis

Fig. 1 showed the results of biochemical analysis. Compared with the control group, the ALT (Fig. 1A), AST (Fig. 1B), TBA (Fig. 1C), TBIL (Fig. 1D) and TG (Fig. 1E) levels were significantly increased ($P < 0.05$) as previous studies[17,23] and the HDL (Fig. 1G) and ALB (Fig. 1I) levels were significantly decreased ($P < 0.05$) in GS-treated groups. Among them, the levels of ALT, AST, TG and ALB changed in a time- and dose-dependent pattern. Serum ALT, AST and TG levels in the high-dose GS-treated groups (H-10 and H-21) were higher than those in the comparative low-dose groups (L-10 and L-21), and their levels in the longer duration exposure groups (L-21 and H-21) were higher than in the comparative shorter duration exposure groups (L-10 and H-10). In contrast, higher serum ALB level was occurred in the low-dose GS-treated group and 10 day groups. In addition, the change of serum TBIL and HDL levels were related to dose. Compared with low-dose groups, the TBIL level was higher and the HDL level was lower in the high-dose groups, respectively. However, there was no obvious and stable change trend in the TCH and LDL levels (Fig. 1F and H).

3.2 Histopathological results

The histopathological results of liver indicated that GS could seriously cause rat liver tissue structure injury. In control group, liver tissues of rat exhibited clear structure, neatly arranged and intact hepatocyte morphology under microscopy (Fig. 2A and D). However, after administration of GS for 10 days, hepatocytes showed disordered arrangement, larger intercellular space, unclear cell boundaries and a small amount of inflammatory

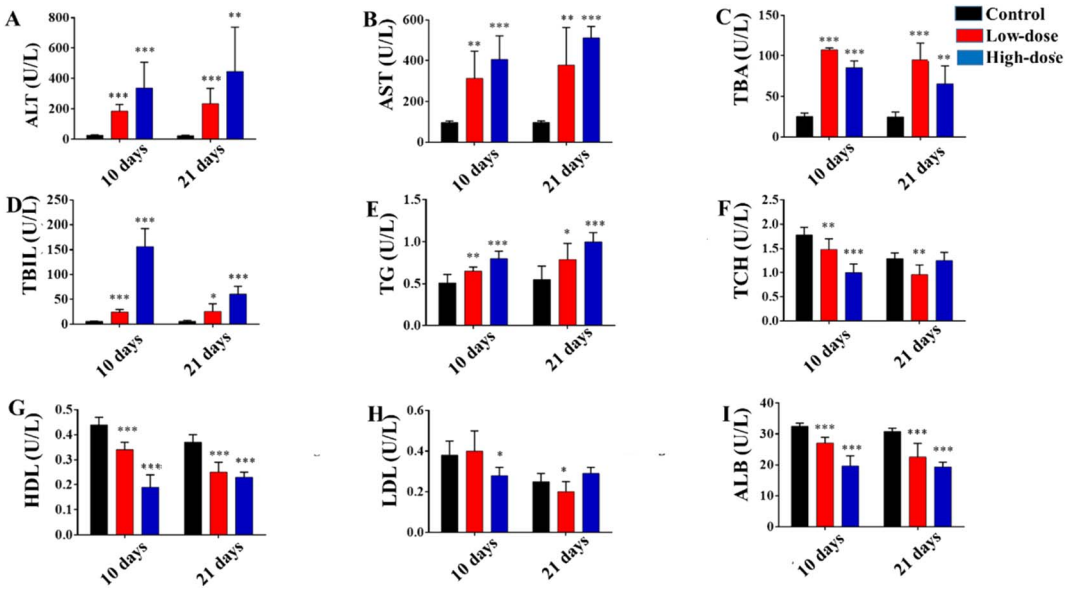

Fig. 1 Biochemical analysis of the effects of *Gynura segetum* after different exposure times and doses by automatic biochemistry analyzer. (A) The level of serum ALT; (B) the level of serum AST; (C) the level of serum TBA; (D) the level of serum TBIL; (E) the level of serum TG; (F) the level of serum TCH; (G) the level of serum HDL; (H) the level of serum LDL; (I) the level of serum ALB. The control group is represented in black, the low-dose group is represented in red, and the high-dose group is represented in blue. *, $P < 0.05$; **, $P < 0.01$; ***, $P < 0.001$, compared with corresponding control group. Values are represented as mean ± SD. ($n = 4–8$).

cell infiltration in the low-dose group (Fig. 2B). Moreover, hemorrhagic necrosis of liver cells was even appeared with the increased dose (Fig. 2C). As the time went, severer hepatocellular cytopathic effect was found in GS-treated groups which the hepatocytes were vacuolated and turbid and cell boundaries were more blurred (Fig. 2E and F). Above results demonstrated the degree of liver tissue structure injury caused by GS was associated with time and dose.

3.3 Multivariate statistical analysis and potential biomarker identification

To investigate the differences of endogenous metabolites in rats at GS-treated group and control group, the PCA analysis was applied to explore the clustering and separation of samples in different groups. After 10 days of administration, the high-dose group was separated from the control group, but low-dose group not (Fig. 3A, $R^2X = 0.676$, $Q^2 = 0.500$). After 21 days of

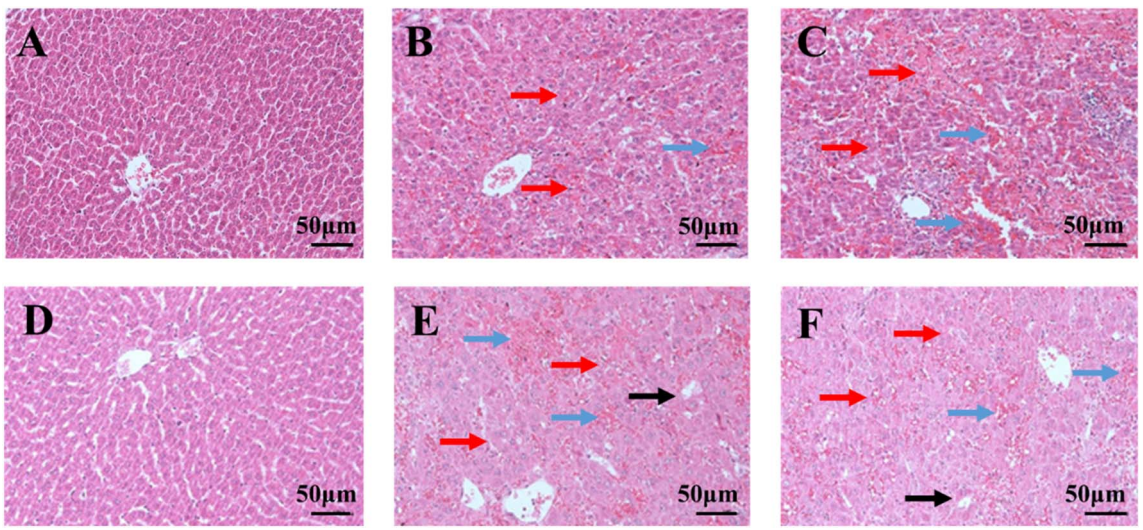

Fig. 2 Hematoxylin and eosin (H&E) staining of liver tissue after different exposure times and doses of *Gynura segetum* (200×). (A) 10 day control group; (B) 10 day low-dose group; (C) 10 day high-dose group; (D) 21 day control group; (E) 21 day low-dose group; (F) 21 day high-dose group. Red arrow represents cell disordered arrangement, blue arrow represents hemorrhagic necrosis and black arrow represents vacuolated hepatocytes.

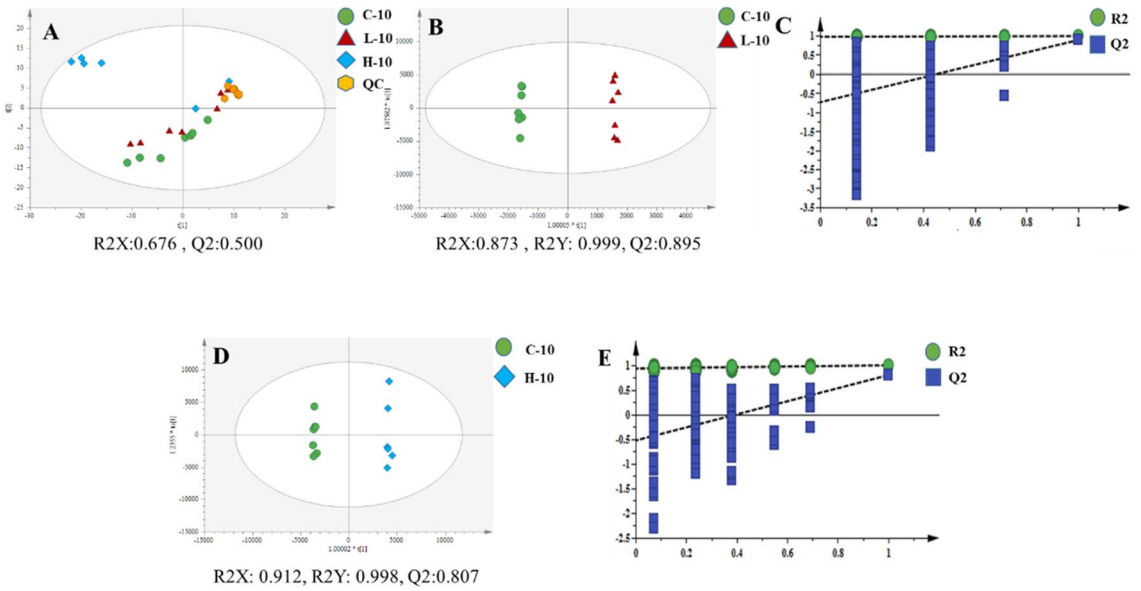

Fig. 3 PCA and OPLS-DA score plot between different groups at 10 days. (A) PCA score plot between control group, low-dose group, high-dose group and QC; (B) OPLS-DA score plot between control group and low-dose group; (D) OPLS-DA score plot between control group and high-dose group. (C-10, 10 day control group; L-10, 10 day low dose group; H-10, 10 day high dose group). The 200-permutation test of OPLS-DA model was for the control and low-dose groups (C) as well as for the control and high-dose groups (E), respectively ($n = 4–8$).

administration, both GS-treated groups were separated from the control group (Fig. 4A, $R^2X = 0.696$, $Q^2 = 0.466$). Meanwhile, these variables had good reproducibility in the whole operational process based on the distribution of QC samples. To observe the trend of change of endogenous metabolites in rats of different GS exposure times and doses, the supervised OPLS-DA was conducted. Finally, the reasonable separation was observed in the OPLS-DA model between GS-treated groups and control group (Fig. 3B: $R^2X = 0.873$, $R^2Y = 0.999$, $Q^2 = 0.895$; Fig. 3D: $R^2X = 0.912$, $R^2Y = 0.998$, $Q^2 = 0.807$; Fig. 4B: $R^2X = 0.933$, $R^2Y = 0.993$, $Q^2 = 0.448$; Fig. 4D: $R^2X = 0.908$, $R^2Y = 0.999$, $Q^2 = 0.687$).

Then 200 iterations-permutation experiments was displayed to substantiate the model (Fig. 3C, E and Fig. 4C, E). Significantly changed metabolites in GS-treated groups were identified based on VIP >1 from the OPLS-DA and $P < 0.05$ from the

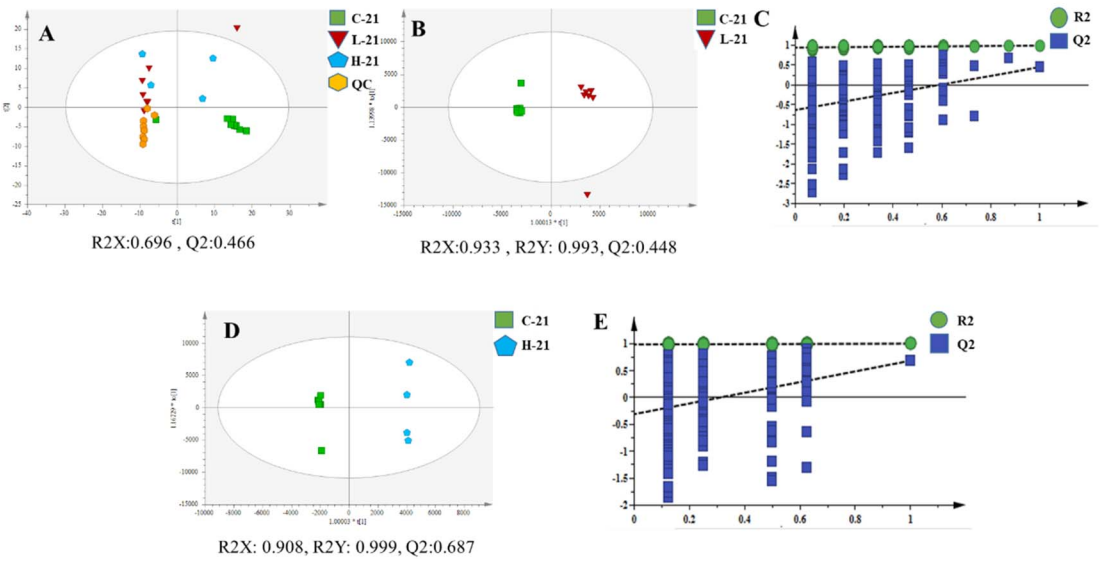

Fig. 4 PCA and OPLS-DA score plot between different groups at 21 days. (A) PCA score plot between control group, low-dose group, high-dose group and QC; (B) OPLS-DA score plot between control group and low-dose group; (D) OPLS-DA score plot between control group and high-dose group. (C-21, 21 day control group; L-21, 21 day low dose group; H-21, 21 day high dose group). The 200-permutation test of OPLS-DA model was for the control and low-dose groups (C) as well as for the control and high-dose groups (E), respectively ($n = 4–8$).

Table 1 Differential metabolites between different groups (GC-MS)

No.	Metabolites	Formula	RT (min)	Mass (m/z)	group	VIP value[a]	P value	FC[b]	Trend
1	Benzene ethanamine	$C_8H_{11}N$	5.89	59.06	L-10 *vs.* C-10	0.782	0.314	1.484	Up
					H-10 *vs.* C-10	0.036	0.947	1.032	Up
					L-21 *vs.* C-21	0.633	0.027	1.857	Up
					H-21 *vs.* C-21	1.255	0.001	2.751	Up
2	D-Lactic acid	$C_3H_6O_3$	7.04	147.00	L-10 *vs.* C-10	1.663	0.510	1.037	Up
					H-10 *vs.* C-10	1.364	0.223	1.075	Up
					L-21 *vs.* C-21	2.622	0.010	1.151	Up
					H-21 *vs.* C-21	3.155	0.016	1.146	Up
3	L-Valine	$C_5H_{11}NO_2$	7.44	72.09	L-10 *vs.* C-10	0.237	0.882	1.048	Up
					H-10 *vs.* C-10	0.792	0.243	0.648	Down
					L-21 *vs.* C-21	2.267	0.000	5.430	Up
					H-21 *vs.* C-21	3.024	0.002	7.235	Up
4	Ethanedioic acid	$C_2H_2O_4$	8.17	147.00	L-10 *vs.* C-10	2.793	0.369	0.715	Down
					H-10 *vs.* C-10	1.214	0.341	0.730	Down
					L-21 *vs.* C-21	4.492	0.002	0.255	Down
					H-21 *vs.* C-21	4.535	0.027	0.362	Down
5	(*R*)-3-Hydroxybutyric acid	$C_4H_8O_3$	8.33	88.01	L-10 *vs.* C-10	1.106	0.034	0.585	Down
					H-10 *vs.* C-10	0.516	0.020	0.538	Down
					L-21 *vs.* C-21	0.876	0.013	0.237	Down
					H-21 *vs.* C-21	0.930	0.070	0.275	Down
6	Urea	CH_4N_2O	9.55	147.00	L-10 *vs.* C-10	3.019	0.577	0.884	Down
					H-10 *vs.* C-10	3.954	0.084	0.617	Down
					L-21 *vs.* C-21	6.507	0.013	0.326	Down
					H-21 *vs.* C-21	3.223	0.393	0.730	Down
7	Serine	$C_3H_7NO_3$	9.68	116.00	L-10 *vs.* C-10	0.924	0.222	0.838	Down
					H-10 *vs.* C-10	0.470	0.198	0.777	Down
					L-21 *vs.* C-21	1.371	0.004	2.214	Up
					H-21 *vs.* C-21	2.042	0.004	2.882	Up
8	L-Isoleucine	$C_6H_{13}NO_2$	9.94	157.99	L-10 *vs.* C-10	0.765	0.611	1.559	Up
					H-10 *vs.* C-10	1.614	0.035	4.523	Up
					L-21 *vs.* C-21	0.269	0.763	0.779	Down
					H-21 *vs.* C-21	0.423	0.637	0.747	Down
9	Acetaldehyde	C_2H_4O	10.03	73.05	L-10 *vs.* C-10	1.565	0.435	0.866	Down
					H-10 *vs.* C-10	2.027	0.125	1.643	Up
					L-21 *vs.* C-21	2.967	0.003	1.697	Up
					H-21 *vs.* C-21	2.723	0.165	1.753	Up
10	Glycine	$C_2H_5NO_2$	10.42	174.00	L-10 *vs.* C-10	0.062	0.967	0.983	Down
					H-10 *vs.* C-10	3.951	0.009	6.290	Up
					L-21 *vs.* C-21	0.237	0.840	0.850	Down
					H-21 *vs.* C-21	0.165	0.901	1.076	Up
11	L-Threonine	$C_4H_9NO_3$	11.44	218.00	L-10 *vs.* C-10	1.472	0.270	1.841	Up
					H-10 *vs.* C-10	2.792	0.012	9.375	Up
					L-21 *vs.* C-21	0.588	0.477	0.605	Down
					H-21 *vs.* C-21	0.143	0.891	0.913	Down
12	Butanoic acid	$C_4H_8O_2$	12.41	243.09	L-10 *vs.* C-10	0.038	0.973	0.982	Down
					H-10 *vs.* C-10	0.533	0.186	1.768	Up
					L-21 *vs.* C-21	1.015	0.008	0.261	Down
					H-21 *vs.* C-21	1.028	0.048	0.387	Down
13	L-Methionine	$C_5H_{11}NO_2S$	13.12	73.04	L-10 *vs.* C-10	0.780	0.730	0.919	Down
					H-10 *vs.* C-10	5.234	0.008	3.950	Up
					L-21 *vs.* C-21	0.764	0.629	1.270	Up
					H-21 *vs.* C-21	2.950	0.039	1.681	Up
14	L-Proline	$C_5H_9NO_2$	13.17	156.00	L-10 *vs.* C-10	0.390	0.810	1.033	Up
					H-10 *vs.* C-10	6.540	0.006	5.841	Up
					L-21 *vs.* C-21	1.526	0.419	1.916	Up
					H-21 *vs.* C-21	3.861	0.015	2.449	Up
15	Alanine	$C_3H_7NO_2$	13.46	120.00	L-10 *vs.* C-10	1.077	0.213	1.892	Up
					H-10 *vs.* C-10	0.407	0.211	1.704	Up
					L-21 *vs.* C-21	2.024	0.000	15.963	Up
					H-21 *vs.* C-21	2.121	0.012	15.482	Up
16	Phenylalanine	$C_9H_{11}NO_2$	14.38	218.00	L-10 *vs.* C-10	1.196	0.128	3.094	Up
					H-10 *vs.* C-10	1.875	0.020	20.593	Up
					L-21 *vs.* C-21	0.764	0.353	6.656	Up

Table 1 (*Contd.*)

No.	Metabolites	Formula	RT (min)	Mass (*m*/*z*)	group	VIP value[a]	*P* value	FC[b]	Trend
					H-21 *vs.* C-21	1.288	0.113	6.956	Up
17	L-Glutamine	$C_5H_{10}N_2O_3$	15.94	73.00	L-10 *vs.* C-10	1.792	0.236	0.772	Down
					H-10 *vs.* C-10	1.142	0.307	1.635	Up
					L-21 *vs.* C-21	1.985	0.007	0.385	Down
					H-21 *vs.* C-21	2.169	0.016	0.480	Down
18	DL-Ornithine	$C_5H_{12}N_2O_2$	16.46	141.99	L-10 *vs.* C-10	2.114	0.097	7.296	Up
					H-10 *vs.* C-10	2.595	0.006	35.702	Up
					L-21 *vs.* C-21	0.646	0.419	4.199	Up
					H-21 *vs.* C-21	0.950	0.235	3.872	Up
19	1,5-Anhydro-D-sorbitol	$C_6H_{12}O_5$	16.82	218.00	L-10 *vs.* C-10	2.152	0.000	0.218	Down
					H-10 *vs.* C-10	0.876	0.000	0.243	Down
					L-21 *vs.* C-21	1.309	0.000	0.186	Down
					H-21 *vs.* C-21	1.435	0.001	0.250	Down
20	L-Sorbose	$C_6H_{12}O_6$	17.14	179.00	L-10 *vs.* C-10	2.412	0.027	2.752	Up
					H-10 *vs.* C-10	1.985	0.004	6.564	Up
					L-21 *vs.* C-21	3.454	0.004	15.451	Up
					H-21 *vs.* C-21	3.655	0.012	13.616	Up
21	D-Allose	$C_6H_{12}O_6$	17.48	160.02	L-10 *vs.* C-10	6.247	0.000	0.781	Down
					H-10 *vs.* C-10	2.648	0.000	0.760	Down
					L-21 *vs.* C-21	3.507	0.000	0.678	Down
					H-21 *vs.* C-21	3.851	0.001	0.719	Down
22	Galactaric acid	$C_6H_{10}O_8$	17.83	333.00	L-10 *vs.* C-10	1.273	0.011	2.701	Up
					H-10 *vs.* C-10	1.101	0.000	6.686	Up
					L-21 *vs.* C-21	0.200	0.265	1.333	Up
					H-21 *vs.* C-21	0.580	0.010	1.965	Up
23	Hexadecanoic acid	$C_{16}H_{32}O_2$	18.49	75.00	L-10 *vs.* C-10	1.367	0.009	0.802	Down
					H-10 *vs.* C-10	0.592	0.039	1.243	Up
					L-21 *vs.* C-21	0.335	0.426	1.196	Up
					H-21 *vs.* C-21	0.051	0.910	1.018	Up
24	*myo*-Inositol	$C_6H_{12}O_6$	19.25	217.00	L-10 *vs.* C-10	1.366	0.007	0.707	Down
					H-10 *vs.* C-10	0.407	0.077	0.787	Down
					L-21 *vs.* C-21	0.769	0.004	0.527	Down
					H-21 *vs.* C-21	0.449	0.287	0.776	Down
25	(*Z*,*Z*)-9,12-Octadecadienoic acid	$C_{18}H_{32}O_2$	20.06	75.00	L-10 *vs.* C-10	1.859	0.022	0.756	Down
					H-10 *vs.* C-10	1.096	0.006	1.406	Up
					L-21 *vs.* C-21	0.830	0.166	1.412	Up
					H-21 *vs.* C-21	0.848	0.198	1.270	Up
26	Cholesterol	$C_{27}H_{46}O$	28.46	129.00	L-10 *vs.* C-10	3.034	0.002	2.270	Up
					H-10 *vs.* C-10	1.187	0.022	2.425	Up
					L-21 *vs.* C-21	0.979	0.004	2.214	Up
					H-21 *vs.* C-21	2.065	0.000	4.085	Up

[a] VIP value was obtained from OPLS-DA. [b] FC (fold change) was calculated as the ratio of the average relative level between two groups. (C-10, 10 day control group; L-10, 10 day low dose group; H-10, 10 day high dose group; C-21, 21 day control group; L-21, 21 day low dose group; H-21, 21 day high dose group) (n = 4–8).

Student's *t*-test, compared with control group. Finally, a total of 26 metabolites were identified by matching with the databases and tentatively regarded as the potential biomarkers in the treated group induced by GS (Table 1). After 10 days of administration, 9 and 12 metabolites were identified from the low-dose group and high-dose group, respectively. And there were 12 and 14 metabolites that were successfully annotated from the low-dose group and high-dose group after 21 days, respectively. The number of metabolites increased with the extension of administration time and the increase of dose. According to the results of metaboanalyst, the related pathway (impact factor >0.1) of those 26 metabolites included linoleic acid metabolism; phenylalanine metabolism; phenylalanine, tyrosine and tryptophan biosynthesis; glycine, serine and threonine metabolism; inositol phosphate metabolism; alanine, aspartate and glutamate metabolism; glyoxylate and dicarboxylate metabolism and cysteine and methionine metabolism (Fig. 5).

3.4 The time- and dose-related differential metabolites in GS induced hepatotoxicity

The Venn diagram (Fig. 6A) was applied to further analyze the significantly differential metabolites in GS-treated groups of different times and doses (L-10, L-21, H-10 and H-21), compared with control group. Interestingly, four clusters were created. There were 2 time- and dose-related metabolites (L-sorbose and D-allose) in cluster I, which changed significantly not only between the different dose groups and control group but also

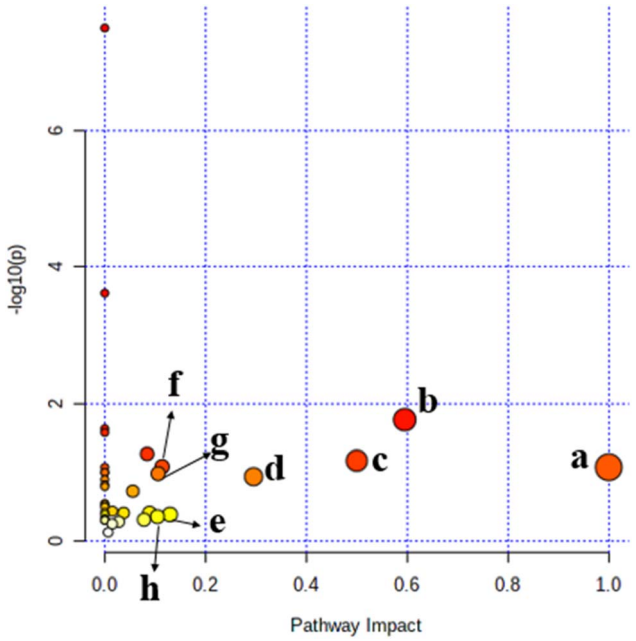

Fig. 5 Summary of metabolic pathway analysis of significantly different metabolites. (a) Linoleic acid metabolism; (b) phenylalanine metabolism; (c) phenylalanine, tyrosine and tryptophan biosynthesis; (d) glycine, serine and threonine metabolism; (e) inositol phosphate metabolism; (f) alanine, aspartate and glutamate metabolism; (g) glyoxylate and dicarboxylate metabolism; (h) cysteine and methionine metabolism.

between the different time groups and control group. Regarding the different dose groups, cluster II showed 2 dose-related metabolites (L-methionine and L-proline) that were unique in the high-dose group, but not in the low-dose group, which might indicate that the hepatotoxicity caused by GS is related to dose. In addition, cluster III and cluster IV represented the unique differential metabolites of the 10 day group (L-10 and H-10) and the 21 day group (L-21 and H-21), respectively. Seven metabolites (D-lactic acid, L-valine, ethanedioic acid, serine, butanoic acid, alanine, and L-glutamine) in 21 day group were more than 2 metabolites (galactaric acid and (*Z*,*Z*)-9,12-octadecadienoic acid) in 10 day group, indicating that they might be time-related metabolites in hepatotoxicity caused by GS.

To directly assess the variation trend of these time- or dose-related differential metabolites levels among various groups, the heat map of 4 clusters were shown in Fig. 6B, respectively. With the extension of administration time and the increase of dose, the level of L-sorbose significantly increased and D-allose significantly decreased in GS-treated groups. Compared with control group, the does-related metabolites L-proline increased in low-dose groups, and further significantly increased in high-dose groups. Moreover, as the time-related metabolites, the content of D-lactic acid and alanine increased after 10 days and further significantly increased after 21 days, while the ethanedioic acid decreased with the extension of time. Meanwhile, the related pathways of 4 clusters were found by Metaboanalyst

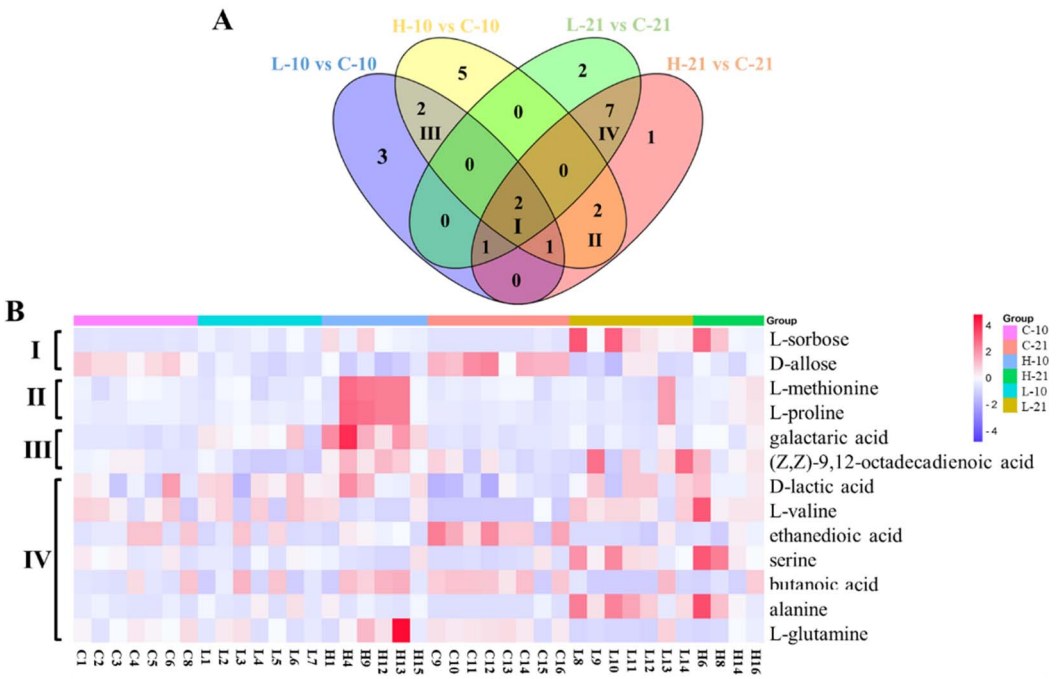

Fig. 6 Venn diagram (A) and heatmaps (B) of significantly different metabolites between different groups. (A) The blue, yellow, green, pink circle represent different metabolites between L-10 group and C-10 group, H-10 group and C-10 group, L-21 group and C-21 group, and H-21 group and C-21 group, respectively. Clusters I–IV illustrated the metabolites that were shared between groups. (B) The heatmaps of 4 clusters of differential metabolites for indicating the impact of *Gynura segetum*. Each row represents a metabolite, and the columns show the expression levels marked with different colors according to the sample type. The red color represents increased metabolites whereas blue color suggests a decrease in content. (C-10, 10 day control group; L-10, 10 day low dose group; H-10, 10 day high dose group; C-21, 21 day control k group; L-21, 21 day low dose group; H-21, 21 day high dose group).

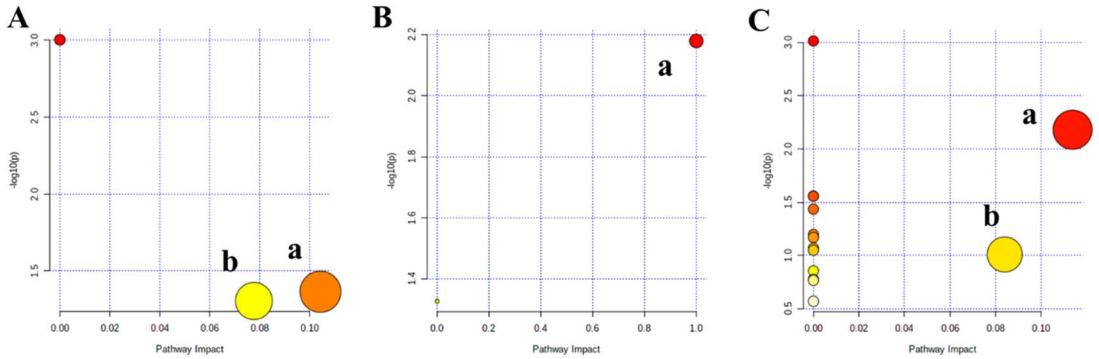

Fig. 7 Metabolic pathway analysis of different metabolites in clusters II–IV. (A) The metabolic pathway of cluster II. (a) Cysteine and methionine metabolism; (b) arginine and proline metabolism; (B) the metabolic pathway of cluster III. (a) Linoleic acid metabolism; (C) the metabolic pathway of cluster IV. (a) Alanine, aspartate and glutamate metabolism; (b) pyruvate metabolism.

(Fig. 7): cluster I was mapped into 0 pathway, cluster II (Fig. 7A) was mapped into 2 pathways (cysteine and methionine metabolism, and arginine and proline metabolism), cluster III (Fig. 7B) were mapped into linoleic acid metabolism and cluster IV (Fig. 7C) were mapped into alanine, aspartate and glutamate metabolism and pyruvate metabolism.

3.5 Correlation analysis between the serum biochemical parameters and differential metabolites

To further understand the correlation of serum biochemical parameters and metabolomic characteristics, we used Spearman correlation analysis to revealed several important associations. The initial data were composed of 9 serum biochemical parameters and 10 significant differential metabolites variables between control and GS-treated groups. As shown in Fig. 8, alanine and cholesterol were positively correlated with ALT, AST, TBA, TBIL and TG but were negatively correlated with HDL and ALB. Interestingly, urea had the opposite results. (*R*)-3-Hydroxybutyric acid had a positive correlation with TCH, HDL and ALB but had a negative correlation with ALT, AST, TBA, TBIL and TG. In addition, *myo*-inositol was positively correlated with TCH, HDL and ALB but was negatively correlated with AST and TBA. D-Lactic acid had a positive correlation with ALT and TBIL, L-proline had a positive correlation with LDL and benzene ethanamine was positively correlated with AST but was negatively correlated with ALB.

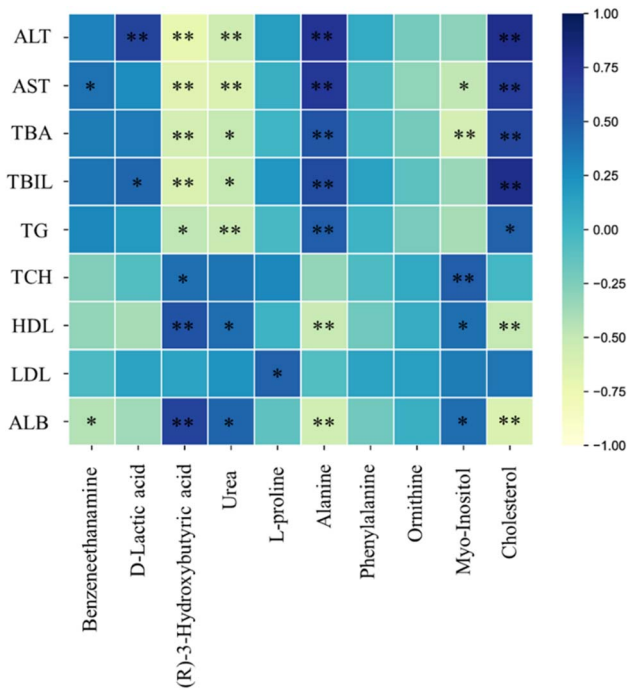

Fig. 8 Heatmaps of correlation analysis between serum biochemical parameters and differential metabolites among the control and GS-treated groups. Blue squares represent positive correlations and yellow squares represent negative correlations. *, $P < 0.05$; **, $P < 0.01$.

4 Discussion

A serum metabolomic method based on GC-MS was established to explicate the toxicity mechanism of different exposure times and doses of GS. *Gynura segetum* (Lour.) Merr is a kind of Chinese folk medicine and the clinical dose range of GS for humans is 3–9 g. However, the hepatotoxicity caused by GS has been reported, and a study summarized the 102 reported HVOD cases caused by GS and found that the individual dose was 150–5000 g, with a median of 500 g.[24] The equivalent dosage in clinic of 7.5 g kg^{-1} in rats for 1 week is just 500 g in human.[22] So we made the animal model of hepatotoxicity of GS with two doses (7.5 g kg^{-1} and 15 g kg^{-1}) according to the previous experiments.[16,25] Since the model effect was not obvious after 7 days, but obvious after 14 days, we explored creatively an intermediate time point (10 day) and a longer time point (21 day). As a result, we also found the occurrence of rats' death after GS administration as previous studies.[22,25] Except that a rat died in 10 day control group due to gavage error, there were 1, 1, 2, 4 rats died because of GS-induced hepatotoxicity in L-10, L-21, H-10 and H-21 groups, respectively. According to previous study, we speculated that the rats death caused by hepatotoxicity might be relevant to time and dose of GS administration. Obviously, the mortality rate of rats was higher in H-21 group

than L-10 group, indicating it's of great significance to explore the relationship between GS-induced hepatotoxicity and the exposure time and dose.

In our study, we found the levels of ALT, AST, TG and ALB significantly changed after GS administration in a time- and dose-dependent pattern while the TBIL and HDL levels altered in a dose-related pattern according to the results of serum biochemical analysis. ALT, AST and ALB are important indexes for clinical manifestation of liver damage.[17] Increased ALT and AST levels indicate that the liver function is damaged, while decreased ALB level is usually associated with the impaired synthetic function of the liver.[26] Additionally, the level of TG in serum reflects the state of lipid metabolism in body.[27] Histopathological examination of liver was further performed to show the liver tissue structure injury by GS-induced hepatotoxicity (Fig. 2). These results suggested that GS might affect liver function and cause hepatotoxicity depending on time and dose. In serum metabolomics analysis, a total of 26 significantly different metabolites were identified and the corresponding 8 metabolic pathways were involved in the GS-treated group, which might interpret hepatotoxicity of GS. The number of metabolites and the levels of time- and dose-related metabolites indicated changes caused by GS in serum endogenous metabolites might be related to time and dose. Moreover, 4 clusters (Fig. 6) were created and related metabolic pathways map (Fig. 7) were drawn, which represented the metabolites and metabolic pathways related to time or dose, respectively. Additionally, strong correlations were found (Fig. 8) between serum biochemical parameters and the differential metabolites based on Spearman's correlation coefficients. Fig. 9 showed the metabolic network of differential metabolites and disturbed metabolic pathways related to hepatotoxicity, which revealed the mechanism of hepatotoxicity induced by GS.

Amino acid metabolism occurs mainly in the liver. When the liver was damaged, the disorder of amino acid metabolism occurred in the body. Interestingly, L-methionine and L-proline were significantly increased in high-dose groups. L-Methionine is necessary for life, but given excessive dietary methionine had increased markers of lipid peroxidation in the liver.[28] Additionally, the abnormal methionine metabolism was related to alcoholic liver disease,[29] and liver toxicity.[30,31] Oxidative stress is a main mechanism underlying hepatotoxicity. And it was reported that cellular proline accumulation was a stress response because proline could scavenge free radical species.[32] Moreover, proline could transform into pyruvate to enter the citrate cycle,[33] which was related to energy metabolism in liver. The increase of valine and serine were as previously reported.[17] Valine is a kind of branched-chain amino acid, which was reported to be crucial for the prevention of liver injury.[34,35] A recent study[36] demonstrated that Ganfule capsule (GFL) might play the protective effect on liver fibrosis by valine biosynthesis. Serine is important in cellular metabolic processes that link glycolysis with one-carbon metabolism to keep redox balance and proliferation.[37] Serine is associated with liver fibrosis[38] and fatty liver disease.[39] Alanine is one of the pyruvate metabolism-related metabolites, playing critical roles in energy metabolism. Glutamine, a traditionally non-essential amino acid, which could improve CCl_4 caused liver fibrosis[40] and prevent alcoholic tissue injury in mouse liver.[41] Glutamine significantly decreased after 21 days, indicating the injury might occur in liver. Phenylalanine could be generated by tyrosine metabolism,[42] and further was oxidized and absorbed by the liver.[43] It has been reported that phenylalanine metabolism disorders were involved in acute liver injury[44] and a higher level of plasma phenylalanine occurred in hepatic disorders,[45] which was similar to our result. L-Ornithine is an important substrate for urea genesis[46] and it could remove toxic ammonia in the liver, exert a hepatoprotective effect by an antioxidative mechanism[47] and treat hepatic encephalopathy.[48] The imbalance of ornithine and urea in our study may indicate the disorders of urea cycle occur in liver.

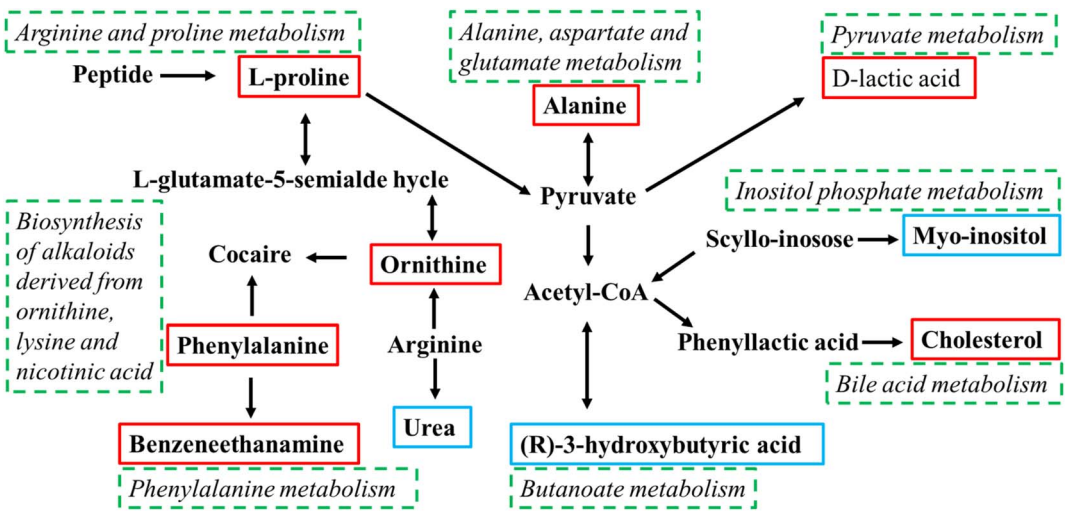

Fig. 9 Schematic diagram of the differential metabolites and disturbed metabolic pathways related to hepatotoxicity induced by GS. The red boxes represent the up-regulated metabolites with significant difference between the control and GS-treated groups, the blue boxes represent the down-regulated metabolites with significant difference between the control and GS-treated groups and the green boxes represent the corresponding metabolic pathways.

The liver is crucial for regulating fatty acid metabolism.[49] Linoleic acid is regarded as regulator and inducer of active oxygen production in fatty liver disease. Meanwhile, linoleic acid is major composition of lipoproteins and phospholipids in the cell membrane.[50] The change of linoleic acid might indicate the hepatotoxicity is related to oxidative stress or lipolysis.[51] After 10 days of administration, linoleic acid changed significantly in GS-treated groups, but not after 21 days. Butanoic acid is a fatty acid and exists as an ester in animal, which produces ATP through mitochondria.[52] The level of butanoic acid decreased significantly in 21 day groups, suggesting the GS-induced hepatotoxicity might be related to energy metabolism. In addition, cholesterol is one of the important lipids. Cholesterol homeostasis is of great significance for synthesis, metabolism, absorption, and excretion of cholesterol.[53] However, an excess of cholesterol in body could be toxic or pathogenic. Accumulation of cholesterol in the liver was associated with hepatotoxicity.[54,55] Interestingly, as a kind of vitamin, *myo*-inositol could prevent the accumulation of lipid in the liver.[56] The hepatic lipids and the lipogenic enzyme activities were deceased[57] and the hepatic triglycerides and cholesterol accumulation were reduced[58] in animals after supplementation of *myo*-inositol. In this study, cholesterol increased and *myo*-inositol decreased in GS-treated groups, which indicated the occurrence of liver damage.

Hepatotoxicity could lead to abnormal carbohydrate metabolism.[59] D-Sorbose and D-allose were both significantly changed in GS-treated groups of different exposure times and doses. D-Sorbose is a rare sugar, which can regulate lipid metabolism by influencing the activity of PAP, the rate-limiting enzyme of triglyceride synthesis.[60] In this study, the sorbose level significantly increased in all GS-treated group, indicating that the mechanism of GS-induced liver toxicity may be related to sugar or lipid metabolism. D-Allose was reported to have protective effect for ischemia/reperfusion injury of the rat liver,[61] the potential inhibitory effect on liver carcinogenesis[62] and the effect of decreasing liver tissue injury levels,[63] which corresponded to the decreased D-allose level in GS-treated groups in our result.

In addition, glycolysis keeps the body's energy requirement when oxygen is insufficient. The level of lactic acid was related to the degree of hepatotoxicity[64] and liver metabolism in HBV (hepatitis B virus)-related ACLF (acute-on-chronic liver failure) patients.[65] The increase level of lactic acid was reported to be associated with the disrupted glycolytic pathway in liver tissues.[66] Ethanedioic acid, one of the metabolites of ethylene glycol (EG), is the cell toxin that harms the central nervous system, heart, lungs and kidneys.[67,68] Primary hyperoxalurias (PHs) is a disorder of liver glyoxylate metabolism with abnormal endogenous oxalate production.[69] In this study, disturbances in lactic acid and ethanedioic acid demonstrated that liver damage may be related to energy metabolism.

In summary, the *Gynura segetum*-induced hepatotoxicity might depend on time and dose. In addition to biochemical indicators, histopathology and changes in serum metabolic profile were related to time and dose by comparison between different time and dose groups. Meanwhile, we found the hepatotoxicity mechanism of different exposure times and doses of GS was related to amino acid metabolism, fatty acid metabolism, carbohydrate metabolism and energy metabolism.

5 Conclusion

In this study, our present experiment was the first to use a serum metabolomics method based on GC-MS for illuminating toxicological mechanisms of different times and doses of GS, which was an important complement to metabolomics study of hepatotoxicity caused by GS. We further explored two new time points of GS administration and found the severe hepatotoxicity occurred at 21 days, and several new metabolites and metabolic pathways related to time and dose of GS were identified. Interestingly, the ALT, AST, TG and ALB were time- and dose-dependent serum biochemical markers in hepatotoxicity of GS. Combining our findings, we concluded that hepatotoxicity caused by GS administration might be associated with time and dose. Our study was helpful for next research on hepatotoxicity caused by GS and clinical application of GS. In conclusion, these results demonstrated that the metabolomics strategy could be a useful tool for toxicity mechanisms and safety evaluation of TCM.

Abbreviations

GS	*Gynura segetum*
SD	Sprague Dawley
ALT	Alanine aminotransferase
AST	Aspartate aminotransferase
TBA	Total bile acid
TBIL	Total bilirubin
TG	Triglycerides
TCH	Total cholesterol
HDL	High-density lipoprotein
LDL	Low-density lipoprotein
ALB	Albumin
ELISA	Enzyme-linked immunosorbent assay
H&E	Hematoxylin and Eosin
GC-MS	Gas chromatography-mass spectrometry
PAs	Pyrrolizidine alkaloids
HSOS	Hepatic sinusoidal obstruction syndrome
UPLC-Q-TOF/MS	Ultraperformance liquid chromatography-quadrupole-time-of-flight/mass spectrometry
LC-MS	Liquid chromatography-mass spectrometry
MMP-9	Matrix metalloproteinase-9
QC	Quality control
PCA	Principal component analysis
OPLS-DA	Orthogonal partial least squares discriminant analysis
VIP	Variable importance for the prediction
FC	Fold-change

Author contributions

Ying Li: investigation, data curation, writing-original draft. Yingxin Tian: investigation, methodology. Qixue Wang; Xinyi

Gu: methodology. Long Chen; Yiqun Jia: investigation, supervision. Shan Cao: investigation, data curation. Ting Zhang: investigation, supervision, writing-review & editing. Mingmei Zhou: investigation, supervision, writing-review & editing, funding acquisition, project administration. Xiaojun Gou: investigation, supervision, funding acquisition, project administration.

Conflicts of interest

The authors declare that they have no conflict of interests regarding this paper.

Acknowledgements

This project was supported by Baoshan District Hospital of Integrated Traditional Chinese and Western Medicine of Shanghai combined with the National Natural Education fund (No. GZRPYJJ-201605) and Innovation Project for Undergraduates of Shanghai University of Traditional Chinese Medicine (202210268241).

References

1 P. Cen, J. Ding and J. Jin, Hepatic sinusoidal obstruction syndrome caused by the ingestion of Gynura segetum in a patient with alcoholic cirrhosis: a case report, *J. Int. Med. Res.*, 2021, **49**(4), 1220780201.

2 M. X. Feng, Y. Shen and Y. Q. Lu, Clinical characteristics and outcomes of patients with hepatic veno-occlusive disease induced by Gynura segetum: A retrospective study, *J. Integr. Med.*, 2020, **18**(5), 434–440.

3 B. R. Zhu, S. B. Pu, D. R. Xu, *et al.*, Advances in Studies on Chemical Constituents and Bioactivities of the Genus Gynura Cass, *Chinese Wild Plant Resources*, 2012, **04**(31), 1–4.

4 L. J. Seow, H. K. Beh, M. I. Umar, *et al.*, Anti-inflammatory and antioxidant activities of the methanol extract of Gynura segetum leaf, *Int. Immunopharmacol.*, 2014, **23**(1), 186–191.

5 G. Lin, J. Y. Wang, N. Li, *et al.*, Hepatic sinusoidal obstruction syndrome associated with consumption of Gynura segetum, *J. Hepatol.*, 2011, **54**(4), 666–673.

6 A. Xiong, F. Yang, L. Fang, *et al.*, Metabolomic and genomic evidence for compromised bile acid homeostasis by senecionine, a hepatotoxic pyrrolizidine alkaloid, *Chem. Res. Toxicol.*, 2014, **27**(5), 775–786.

7 P. Richardson and E. Guinan, The pathology, diagnosis, and treatment of hepatic veno-occlusive disease: current status and novel approaches, *Br. J. Haematol.*, 1999, **107**(3), 485–493.

8 Y. Wang, D. Qiao, Y. Li, *et al.*, Risk factors for hepatic veno-occlusive disease caused by Gynura segetum: a retrospective study, *BMC Gastroenterol.*, 2018, **18**(1), 156.

9 P. Ou, X. Liu, Z. Tang, *et al.*, Gynura Segetum Related Hepatic Sinusoidal Obstruction Syndrome: A Liver Disease with High Mortality and Misdiagnosis Rate, *Curr. Pharm. Des.*, 2019, **25**(35), 3762–3768.

10 P. P. Fu, Q. Xia, G. Lin, *et al.*, Pyrrolizidine alkaloids-genotoxicity, metabolism enzymes, metabolic activation, and mechanisms, *Drug Metab. Rev.*, 2004, **36**(1), 1–55.

11 L. Ji, T. Liu and Z. Wang, Pyrrolizidine alkaloid clivorine induced oxidative injury on primary cultured rat hepatocytes, *Hum. Exp. Toxicol.*, 2010, **29**(4), 303–309.

12 D. P. Li, Y. L. Chen, H. Y. Jiang, *et al.*, Phosphocreatine attenuates Gynura segetum-induced hepatocyte apoptosis *via* a SIRT3-SOD2-mitochondrial reactive oxygen species pathway, *Drug Des., Dev. Ther.*, 2019, **13**, 2081–2096.

13 X. Z. Yu, T. Ji, X. L. Bai, *et al.*, Expression of MMP-9 in hepatic sinusoidal obstruction syndrome induced by Gynura segetum, *J. Zhejiang Univ., Sci., B*, 2013, **14**(1), 68–75.

14 W. Zhang, L. Zhou, P. Yin, *et al.*, A weighted relative difference accumulation algorithm for dynamic metabolomics data: long-term elevated bile acids are risk factors for hepatocellular carcinoma, *Sci. Rep.*, 2015, **5**, 8984.

15 K. Zaitsu, Y. Hayashi, M. Kusano, *et al.*, Application of metabolomics to toxicology of drugs of abuse: A mini review of metabolomics approach to acute and chronic toxicity studies, *Drug Metab. Pharmacokinet.*, 2016, **31**(1), 21–26.

16 S. Qiu, H. Zhang, Q. Fei, *et al.*, Urine and plasma metabolomics study on potential hepatoxic biomarkers identification in rats induced by Gynura segetum, *J. Ethnopharmacol.*, 2018, **216**, 37–46.

17 X. L. Wang, X. J. Gou, L. Chen, *et al.*, Metabolomics of Gynura segetum-induced hepatotoxicity in rats, *Chin. Tradit. Pat. Med.*, 2019, **08**(41), 1826–1834.

18 M. R. Zhan, X. J. Gou, L. Chen, *et al.*, Mechanism study on Gynura segetum induced liver injury in rats based on urine metabonomics, *Acad. J. Shanghai Univ. Tradit. Chin. Med.*, 2019, **01**(33), 60–65.

19 A. Zhang, H. Sun, P. Wang, *et al.*, Modern analytical techniques in metabolomics analysis, *Analyst*, 2012, **137**(2), 293–300.

20 A. Mastrangelo, A. Ferrarini, F. Rey-Stolle, *et al.*, From sample treatment to biomarker discovery: A tutorial for untargeted metabolomics based on GC-(EI)-Q-MS, *Anal. Chim. Acta*, 2015, **900**, 21–35.

21 G. A. Gowda and D. Djukovic, Overview of mass spectrometry-based metabolomics: opportunities and challenges, *Methods Mol. Biol.*, 2014, **1198**, 3–12.

22 Y. Song, Z. Yu, Y. H. Fan, *et al.*, A rat model of hepatic veno-occlusive disease induced by the Gynura root water decoction, *J. Clin. Exp. Hepatol.*, 2011, **08**(27), 860–864.

23 Y. H. Li, X. J. Gou, L. Chen, *et al.*, Targeted metabonomics study of serum bile acid in rats with hepatotoxicity induced by Gynura segetum, *Chin. Tradit. Pat. Med.*, 2021, **09**(43), 2539–2544.

24 Y. Song and Y. H. Fan, Clinical features of hepatic veno-occlusive disease induced by gynura root: analysis of 102 cases, *J. Clin. Exp. Hepatol.*, 2011, **27**(05), 496–499.

25 X. J. Gou, J. M. Cao and L. X. Hou, Research on rat model of hepatic veno-occlusive disease induced by Gynura Segetum, *Acad. J. Shanghai Univ. Tradit. Chin. Med.*, 2017, **31**(05), 86–90.

26 Y. Wu, H. Li, X. Guo, *et al.*, Incidence, risk factors, and prognosis of abnormal liver biochemical tests in COVID-19 patients: a systematic review and meta-analysis, *Hepatol. Int.*, 2020, **14**(5), 621–637.
27 G. W. Wang, X. L. Zhang, Q. H. Wu, *et al.*, The hepatoprotective effects of Sedum sarmentosum extract and its isolated major constituent through Nrf2 activation and NF-kappaB inhibition, *Phytomedicine*, 2019, **53**, 263–273.
28 W. C. Sim, H. Q. Yin, H. S. Choi, *et al.*, L-serine supplementation attenuates alcoholic fatty liver by enhancing homocysteine metabolism in mice and rats, *J. Nutr.*, 2015, **145**(2), 260–267.
29 M. Jia, Y. Wang, M. Teng, *et al.*, Toxicity and metabolomics study of isocarbophos in adult zebrafish (Danio rerio), *Ecotoxicol. Environ. Saf.*, 2018, **163**, 1–6.
30 A. S. Meena, P. K. Shukla, P. Sheth, *et al.*, EGF receptor plays a role in the mechanism of glutamine-mediated prevention of alcohol-induced gut barrier dysfunction and liver injury, *J. Nutr. Biochem.*, 2019, **64**, 128–143.
31 R. Rodriguez-Agudo, N. Goikoetxea-Usandizaga, M. Serrano-Macia, *et al.*, Methionine Cycle Rewiring by Targeting miR-873-5p Modulates Ammonia Metabolism to Protect the Liver from Acetaminophen, *Antioxidants*, 2022, **11**(5), 897.
32 C. Hu, R. Li, J. Wang, *et al.*, Untargeted metabolite profiling of liver in mice exposed to 2-methylfuran, *J. Food Sci.*, 2021, **86**(1), 242–250.
33 Y. Li, G. Lin, B. Chen, *et al.*, Effect of alprazolam on rat serum metabolic profiles, *Biomed. Chromatogr.*, 2017, **31**(9), e3956.
34 Y. Nagata, N. Mizuta, A. Kanasaki, *et al.*, Rare sugars, d-allulose, d-tagatose and d-sorbose, differently modulate lipid metabolism in rats, *J. Sci. Food Agric.*, 2018, **98**(5), 2020–2026.
35 A. Miura, T. Hosono and T. Seki, Macrophage potentiates the recovery of liver zonation and metabolic function after acute liver injury, *Sci. Rep.*, 2021, **11**(1), 9730.
36 C. Ke, J. Gao, J. Tu, *et al.*, Ganfule capsule alleviates bile duct ligation-induced liver fibrosis in mice by inhibiting glutamine metabolism, *Front. Pharmacol.*, 2022, **13**, 930785.
37 M. A. Hossain, K. Izuishi, M. Tokuda, *et al.*, D-Allose has a strong suppressive effect against ischemia/reperfusion injury: a comparative study with allopurinol and superoxide dismutase, *J. Hepatobiliary Pancreat. Sci.*, 2004, **11**(3), 181–189.
38 M. Yokohira, K. Hosokawa, K. Yamakawa, *et al.*, Potential inhibitory effects of D-allose, a rare sugar, on liver preneoplastic lesion development in F344 rat medium-term bioassay, *J. Biosci. Bioeng.*, 2008, **105**(5), 545–553.
39 M. A. Hossain, H. Wakabayashi, K. Izuishi, *et al.*, Improved microcirculatory effect of D-allose on hepatic ischemia reperfusion following partial hepatectomy in cirrhotic rat liver, *J. Biosci. Bioeng.*, 2006, **101**(4), 369–371.
40 W. Chen, J. You, J. Chen, *et al.*, Combining the serum lactic acid level and the lactate clearance rate into the CLIF-SOFA score for evaluating the short-term prognosis of HBV-related ACLF patients, *Expert Rev. Gastroenterol. Hepatol.*, 2020, **14**(6), 483–489.
41 C. Shi, X. Han, X. Mao, *et al.*, Metabolic profiling of liver tissues in mice after instillation of fine particulate matter, *Sci. Total Environ.*, 2019, **696**, 133974.
42 F. Valdivieso, C. Gimenez and F. Mayor, In vivo inhibition of rat liver phenylalanine hydroxylase by p-chlorophenylalanine and Esculin. Experimental model of phenylketonuria, *Biochem. Med.*, 1975, **12**(1), 72–78.
43 A. Ito, T. Kohno, I. Hosoi, *et al.*, High correlation between results of the [1-13C]-phenylalanine breath test and phenylalanine hydroxylase (EC 1.14.16.1) activity of the liver in rats, *Digestion*, 2001, **63**(2), 130–138.
44 Y. Yan, N. Shi, X. Han, *et al.*, UPLC/MS/MS-Based Metabolomics Study of the Hepatotoxicity and Nephrotoxicity in Rats Induced by Polygonum multiflorum Thunb, *ACS Omega*, 2020, **5**(18), 10489–10500.
45 R. Barazzoni, M. Zanetti, M. Vettore, *et al.*, Relationships between phenylalanine hydroxylation and plasma aromatic amino acid concentrations in humans, *Metabolism*, 1998, **47**(6), 669–674.
46 L. B. Vong, Y. Ibayashi, Y. Lee, *et al.*, Poly(ornithine)-based self-assembling drug for recovery of hyperammonemia and damage in acute liver injury, *J. Controlled Release*, 2019, **310**, 74–81.
47 A. K. Najmi, K. K. Pillai, S. N. Pal, *et al.*, Effect of l-ornithine l-aspartate against thioacetamide-induced hepatic damage in rats, *Indian J. Pharmacol.*, 2010, **42**(6), 384–387.
48 H. Uchisawa, A. Sato, J. Ichita, *et al.*, Influence of low-temperature processing of the brackish-water bivalve, Corbicula japonica, on the ornithine content of its extract, *Biosci., Biotechnol., Biochem.*, 2004, **68**(6), 1228–1234.
49 E. Letavernier and M. Daudon, Stiripentol identifies a therapeutic target to reduce oxaluria, *Curr. Opin. Nephrol. Hypertens.*, 2020, **29**(4), 394–399.
50 P. M. Leth and M. Gregersen, Ethylene glycol poisoning, *Forensic Sci. Int.*, 2005, **155**(2–3), 179–184.
51 S. Xu, F. Kong, Z. Sun, *et al.*, Hepatoprotective effect and metabonomics studies of radix gentianae in rats with acute liver injury, *Pharm. Biol.*, 2021, **59**(1), 1172–1180.
52 M. Dindo, C. Conter, E. Oppici, *et al.*, Molecular basis of primary hyperoxaluria: clues to innovative treatments, *Urolithiasis*, 2019, **47**(1), 67–78.
53 J. Pearce, The effects of choline and inositol on hepatic lipid metabolism and the incidence of the fatty liver and kidney syndrome in broilers, *Br. Poult. Sci.*, 1975, **16**(6), 565–570.
54 Y. Okazaki and T. Katayama, Effects of dietary carbohydrate and *myo*-inositol on metabolic changes in rats fed 1,1,1-trichloro-2,2-bis (p-chlorophenyl) ethane (DDT), *J. Nutr. Biochem.*, 2003, **14**(2), 81–89.
55 K. Roth, Z. Yang, M. Agarwal, *et al.*, Exposure to a mixture of legacy, alternative, and replacement per- and polyfluoroalkyl substances (PFAS) results in sex-dependent modulation of cholesterol metabolism and liver injury, *Environ. Int.*, 2021, **157**, 106843.
56 A. Pani, R. Giossi, D. Menichelli, *et al.*, Inositol and Non-Alcoholic Fatty Liver Disease: A Systematic Review on Deficiencies and Supplementation, *Nutrients*, 2020, **12**(11), 3379.

57 F. R. Maxfield and I. Tabas, Role of cholesterol and lipid organization in disease, *Nature*, 2005, **438**(7068), 612–621.
58 X. Wang, X. Fu, C. Van Ness, *et al.*, Bile Acid Receptors and Liver Cancer, *Curr. Pathobiol. Rep.*, 2013, **1**(1), 29–35.
59 N. Mori and K. Hirayama, Long-term consumption of a methionine-supplemented diet increases iron and lipid peroxide levels in rat liver, *J. Nutr.*, 2000, **130**(9), 2349–2355.
60 C. H. Halsted, J. A. Villanueva, A. M. Devlin, *et al.*, Folate deficiency disturbs hepatic methionine metabolism and promotes liver injury in the ethanol-fed micropig, *Proc. Natl. Acad. Sci. U. S. A.*, 2002, **99**(15), 10072–10077.
61 J. D. Finkelstein, Methionine metabolism in liver diseases, *Am. J. Clin. Nutr.*, 2003, **77**(5), 1094–1095.
62 J. T. Dever and A. A. Elfarra, L-methionine toxicity in freshly isolated mouse hepatocytes is gender-dependent and mediated in part by transamination, *J. Pharmacol. Exp. Ther.*, 2008, **326**(3), 809–817.
63 Y. Obayashi, H. Arisaka, S. Yoshida, *et al.*, Proline protects liver from D-galactosamine hepatitis by activating the IL-6/STAT3 survival signaling pathway, *Amino Acids*, 2012, **43**(6), 2371–2380.
64 R. Heidari, H. Mohammadi, V. Ghanbarinejad, *et al.*, Proline supplementation mitigates the early stage of liver injury in bile duct ligated rats, *J. Basic Clin. Physiol. Pharmacol.*, 2018, **30**(1), 91–101.
65 H. Cui, Y. Li, M. Cao, *et al.*, Untargeted Metabolomic Analysis of the Effects and Mechanism of Nuciferine Treatment on Rats With Nonalcoholic Fatty Liver Disease, *Front. Pharmacol.*, 2020, **11**, 858.
66 C. R. Green, M. Wallace, A. S. Divakaruni, *et al.*, Branched-chain amino acid catabolism fuels adipocyte differentiation and lipogenesis, *Nat. Chem. Biol.*, 2016, **12**(1), 15–21.
67 K. Tajiri and Y. Shimizu, Branched-chain amino acids in liver diseases, *World J. Gastroenterol.*, 2013, **19**(43), 7620–7629.
68 W. C. Sim, W. Lee, H. Sim, *et al.*, Downregulation of PHGDH expression and hepatic serine level contribute to the development of fatty liver disease, *Metabolism*, 2020, **102**, 154000.
69 H. H. Yun, S. Park, M. J. Chung, *et al.*, Effects of losartan and l-serine in a mouse liver fibrosis model, *Life Sci.*, 2021, **278**, 119578.